Formation of vacancy-impurity complexes by annealing elementary vacancies introduced by electron irradiation of As-, P-, and Sb-doped Si

V. Ranki, A. Pelli, and K. Saarinen
Laboratory of Physics, Helsinki University of Technology, P. O. Box 1100, FIN-02015 HUT, Finland
(Received 13 October 2003; revised manuscript received 12 December 2003; published 12 March 2004)

Positron annihilation experiments have been performed to identify defects created by annealing of electron irradiated of heavily As-, P-, and Sb-doped Si samples. We show that the vacancy-donor pairs (V-D_1) migrate around 450 K, transforming into V-D_2 defects. These defects turn into V-D_3 around 700 K provided the doping concentration is high enough. We furthermore show that the V-As_3 defects anneal at 1100 K. The formation and annealing of these defects can explain the observed electrical compensation and activation in highly doped Si. We also show that the deconvoluted valence region of the positron-electron momentum distribution can be used to identify atoms neighboring a vacancy and that the chemical effects of individual atoms can be extracted from the momentum distribution.

DOI: 10.1103/PhysRevB.69.115205 PACS number(s): 61.72.−y, 61.82.Fk, 66.30.−h, 78.70.Bj

I. INTRODUCTION

When Si is doped to concentrations above $\sim 3 \times 10^{20}$ cm^{-3}, fundamental material problems start to appear. The free-carrier concentration saturates to this value both in donor-implanted[1] and molecular-beam epitaxy (MBE)-grown[2,3] Si. As the deactivation takes place, also enhanced donor diffusion is observed, indicating that a new migration mechanism becomes dominant.[4]

The reason for the electrical deactivation is believed to be a defect complex, the formation of which is also related to the observed enhanced donor diffusion. One suggested group of defects are the precipitates which have been observed in Si subjected to high-temperature (700–1000 °C) annealing.[1,5,6] The most discussed defect complexes are, however, vacancy-donor complexes, where one or several Si vacancies are surrounded by one or more donor atoms at substitutional sites (V_m-D_n).

Theoretical calculations show that the formation energies of V-D_n decrease with increasing n and with $n>2$ they become negative, suggesting that defects with high n should be abundantly present at all doping levels.[7,8] Thus also the electrical deactivation should happen at all concentrations. This is, however, not observed, which is usually explained by kinetic processes limiting the formation of V-D_n.

Mathiot and Pfister have suggested that the enhanced diffusion happens by a percolation model provided the donor concentration is high enough.[9] The donor atoms form an infinite cluster when they are fifth nearest neighbors or closer to each other. Then the vacancies which are third nearest neighbor to a donor can be second nearest to another donor, thus lowering the migration barrier of the donor atoms. Later it was proposed that it is enough that the donor atoms are ninth nearest neighbors and also that larger complexes (V-D_2) can diffuse with similar mechanisms.[8,10] The migration barrier of V-D_2 (2.0 eV for V-As_2) is, however, larger than for V-D_1 (1.19 eV for V-As_1) and thus happens only at larger temperatures.[10] Further theoretical proof for the electrical deactivation by vacancy-donor complexes has been presented by Berding and Sher in a form of electronic quasichemical formalism calculations which indicate that V-As_n complexes with high n are responsible for the deactivation.[11]

There is also experimental evidence which gives proof that vacancy-donor complexes are responsible for the observed electrical compensation and enhanced diffusion. Isoconcentration measurements by Nylandsted Larsen *et al.*, suggest that V-Sb_1 and V-Sb_2 are responsible for the diffusion in highly Sb-doped Si.[12] Theoretical calculations and extended x-ray-absorption fine-structure measurements (EXAFS) by Pandey *et al.* suggest that V-As_4 complex plays a strong role in the deactivation in highly As-doped Si.[7] They note, however, that smaller defects, such as V-As_3, have not been considered and they can also play a role in the deactivation.

Highly doped Si was studied with positrons earlier. Lawther *et al.* found evidence that V-As_n complexes (with average n being greater than 2) are associated to the electrical deactivation in highly As-doped Si.[13] Myler *et al.* have studied Si($[As]=4\times10^{20}$ cm^{-3}) using a two-detector coincidence system.[14] They observed an increase in As signal after 500 and 750 °C annealings, indicating the formation of V-As_n defects. Szpala *et al.* have made coincidence Doppler measurements on highly Sb-doped Si (up to 2.4×10^{21} cm^{-3}).[15] They studied the effect of Sb to the core region of the electron momentum distribution and proposed that a single Sb bound to a vacancy is the compensating acceptor in highly doped material.

In addition to the vacancy-donor complexes, other defects have been considered as well. Based on first-principles calculations and x-ray-absorption measurements, Chadi *et al.* have proposed a donor-pair defect as being responsible for the deactivation in highly Sb-doped Si.[16] These defects contain two separated but interacting dopant atoms with no associated Si vacancies. In later measurements by an annular dark-field scanning transmission electron microscope by Voyles *et al.*, direct evidence of Sb pairs was obtained but it was impossible to discriminate between the donor-pair and V-Sb_2 defects.[17,18]

Information related to the electrical deactivation at high doping levels has also been obtained from measurements in

Si where vacancies have been created artificially by electron irradiation. By observing the defect migrations and formations in electron-irradiated Si during annealings, one gains information about processes taking place during the growth of Si. Since the vacancy is mobile well below room temperature, it can survive temperatures at and above room temperature only as trapped at some defect, such as at a neighboring site of a donor atom. Watkins *et al.* have identified the V-D_1 defects formed by electron irradiation in P-, As-, and Sb-doped Si using electron paramagnetic resonance (EPR) and electron-nuclear double resonance (ENDOR).[19,20] They also found that these defects anneal at relatively low temperatures.

Positrons have also been applied to study electron-irradiated Si. Mäkinen *et al.* have investigated Si($[\mathrm{P}] = 10^{20}$ cm^{-3}) using positron lifetime measurements to show that positrons are trapped at V-P_1 defects.[21,22] The annealing of V-D_1 defects in P-, As-, and Sb-doped Si have been studied by Polity *et al.*[23] They found that the V-D_1 defects annealed at temperatures around 400–450 K. They also found divacancies which annealed between 500 and 650 K. Avalos and Dannefaer have studied P- and Sb-doped samples with concentrations between 10^{16} and 5×10^{18} cm^{-3}.[24] Their conclusion was that at lower doping V_2-D_1 defects dominate whereas at dopings around 5×10^{18} cm^{-3} the V-D_1 is the dominant defect.

In our earlier positron annihilation experiments, we found that V-As_3 defects are present in small concentrations in Czochralski-grown Si($[\mathrm{As}]=10^{20}$ cm^{-3}) samples.[25] We further showed that these defects are formed at high concentrations by annealing of electron irradiated samples with the same As concentration.[26] We observed that V-As_1 defects formed by the electron irradiation start to migrate at around 450 K, forming V-As_2 defects. These defects in turn transform to V-As_3 defects at 700 K. It was seen that the formations of the larger V-As_2 and V-As_3 defects depend heavily on the As concentration. These observations explain the enhanced diffusion caused by the migration of V-As_1 and V-As_2 and also the deactivation caused by stable V-As_3 at high As concentrations.

We have also found V-As_3 (and also V_2-As_5) defects in MBE-grown Si$[[\mathrm{As}]=(1.5\text{–}3.5)\times10^{20}$ cm$^{-3}]$ where As doping is done by implantation. The defect concentrations reach almost 10^{20} cm^{-3},[27] which is high enough to be responsible for the observed deactivation. We found that the defects anneal at 800 and 900 °C, respectively, together with the electrical activation of As. It was also seen that the greatest free-carrier concentration is obtained with the shortest cooling time after the annealing, demonstrating the importance of the kinetics of the cluster formation.

In this paper, we continue the measurements on electron-irradiated Czochralski-grown Si samples. We will show that similar diffusion mechanisms and defects complexes, as was found in As-doped samples, are also present in P- and Sb-doped Si. We perform theoretical calculations to strengthen the interpretation of the positron annihilation measurements. We also take advantage of positron data analysis methods including deconvolution of the valence region electron momentum distribution and division of the momentum distribution to contributions from individual Si and donor atoms.

TABLE I. Doping concentrations (n), electron irradiation energies (E_e), and irradiation doses (ϕ_e) of the measured samples.

Dopant	n (cm^{-3})	E_{e^-} (MeV)	ϕ_e (cm^{-2})
As	10^{19}		
As	10^{20}		
As	10^{19}	2	1×10^{18}
As	10^{20}	2	5×10^{18}
P	3×10^{16}	2	2×10^{16}
P	10^{20}	2.5	5×10^{17}
Sb	3×10^{18}	2	3×10^{17}
Sb	3×10^{18}	2	1×10^{18}
Sb	3×10^{18}	2	2.8×10^{18}

II. METHOD

A. Experiment

We performed both positron lifetime and coincidence Doppler measurements in order to identify the defects in highly doped silicon at different stages of the annealing procedure. The lifetime measurements were performed using a conventional fast-fast coincidence system with a time resolution of 230 ps. A 30 μCi ^{22}Na source was sandwiched between two identical sample pieces. The effect of positrons annihilating in the source material and the aluminum foil surrounding it were removed by measuring a well-known reference sample where these source corrections can be easily determined. The corrections were 215 ps (2.1%), 400 ps (2.7%), and 1500 ps (0.09%). For more details, see Ref. 28.

The Doppler broadening of the annihilation radiation was measured using a coincidence system with two Ge detectors. Both of the 511-keV photons emitted from the e^+-e^- annihilation were detected using the Ge detectors and a two-parameter multichannel analyzer. The annihilation events were recorded in a two-dimensional matrix by adding a count to the matrix element defined by the observed energies of the annihilation photons. Due to momentum and energy conservation, true annihilation events go to the diagonal of the matrix from where the one-dimensional electron momentum distribution can be obtained. From the other diagonal, the resolution of the measurements system can be obtained. An energy resolution of 0.95 keV and a peak-to-background ratio of 2×10^6 were achieved.

B. Measured samples

We studied several Czochralski-grown Si(111) bulk crystals with different As-, P-, and Sb-doping concentrations. Most of the samples were irradiated at 300 K with 2-MeV electrons in order to create vacancy defects above thermal equilibrium concentration. The donor concentrations and electron-irradiation doses are shown in Table I.

After electron irradiation, the samples were annealed isochronally (30 min) in vacuum (10^{-3} mbar) at 300–1220 K and between the annealings positron lifetime measurements

were conducted at room temperature. In the case of Si([P] $=3\times10^{16}$ cm^{-3}), measurements were made also at lower temperatures in order to take advantage of the enhanced positron trapping.[21,22,29] When there were significant changes in the positron lifetime, we performed coincidence Doppler-broadening measurements with two Ge detectors at room temperature.

III. DATA ANALYSIS

A. Deconvolution of the momentum distribution

1. Deconvolution procedure

In order to study the low momentum valence region of the electron momentum distribution, the spectra were deconvoluted with the resolution function of the two-parameter system. The resolution for each measurement was obtained individually from the 1022-keV (E_1+E_2) axis of the two-dimensional Doppler spectrum. The resolution function was found to represent a Gaussian function with high precision.

The deconvolution was made with the model-independent unfolding method.[30] The detected spectrum $\boldsymbol{C}$ can be written as a matrix equation $\boldsymbol{C}=\boldsymbol{WR}$, where $\boldsymbol{W}$ is the original spectrum and $\boldsymbol{R}$ is the resolution matrix. If $\boldsymbol{R}^{-1}$ is known, then the original spectrum can be obtained as $\boldsymbol{W}=\boldsymbol{CR}^{-1}$. Since the inversion of a large matrix is difficult, an iterative procedure without matrix inversion was used as in Ref. 30.

The convergence of the iteration can be tested by calculating the norm S_N of the difference between the convoluted Nth iteration and the measured distribution. By increasing the number of iterations, the S_N gets smaller but also the noise in the original measured distribution becomes more visible. The noise can be reduced somewhat by averaging adjacent points. A compromise between the S_N and the noise level needs to be made, and in these measurements the fifth iteration was found to give the best results in terms of both convergence and noise.

2. Comparison with angular correlation experiments

In order to test the validity of the deconvolution, momentum distributions measured in defect-free [100] and [111] Si were compared to one-dimensional angular correlation of annihilation radiation (1D-ACAR) measurements[31] and theoretical calculations.[32] These distributions are shown in Fig. 1. Backgrounds have been removed and the measured spectra have been normalized to make comparison possible.

As can be seen from the figure, the 1D-ACAR and the deconvoluted Doppler-broadening measurements agree very well with each other, making the deconvolution process plausible. Also the agreement with the theoretical distribution is very good, although slightly worse than between the 1D-ACAR and Doppler measurements.

B. Element-specific momentum distributions

The Doppler-broadening experiments yield chemical information on the atoms at the positron annihilation site. Hence, it has been suggested that the Doppler-broadening curves could be constructed of element-specific momentum distributions which could be recorded in reference samples.[15,33,34] However, it is questionable whether such a superposition could always be justified, since the positron state and lattice symmetry of the reference material could be very different from those in the studied sample. On the other hand, at different vacancy-impurity complexes the trapped positron state is always very similar, and thus the recorded momentum distribution can be successfully decomposed to element-specific constituents, as will be shown below.

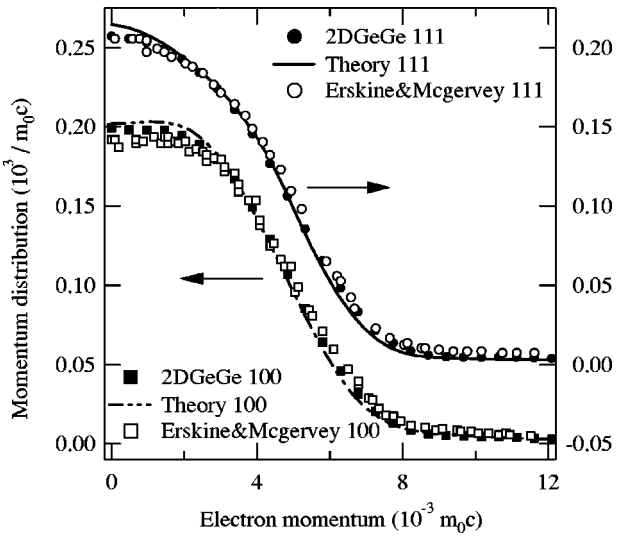

FIG. 1. Electron momentum distributions in defect-free [100] and [111] Si from deconvoluted two Ge detector coincidence measurements, 1D-ACAR measurements (Ref. 31), and theoretical calculations (Ref. 32).

The momentum distribution $\rho(\boldsymbol{p})$ of the annihilation radiation can be written as

$$\rho(\boldsymbol{p})=\frac{\pi r_0 c}{V}\sum_h \left|\int d\boldsymbol{r} e^{-i\boldsymbol{p}\cdot\boldsymbol{r}}\psi_+(\boldsymbol{r})\psi_h(\boldsymbol{r})\sqrt{\gamma_h(\boldsymbol{r})}\right|^2, \quad (1)$$

where ψ_+ and ψ_h are the positron and electron wave functions, respectively. Thus the momentum distribution of a vacancy can be written as a sum of distributions from different atoms, namely

$$\rho=\sum_{i'=1}^{k'}\rho_{i'}=\sum_{i=1}^{k}\rho_i+\sum_{j=k+1}^{k'}\rho_j, \quad (2)$$

where k' is the number of atoms in the system and k the number of nearest neighbors of the vacancy. If we assume that the second nearest neighbors and further atoms are similar to those of the ideal lattice and that they see the same positron wave function regardless of the atoms neighboring the vacancy, we can approximate the latter sum in Eq. (2) with a constant A. If there are m different kinds of atoms as nearest neighbors with n_i atoms of each chemical type ($\Sigma_{i=1}^{m}n_i=k$), we can write the distribution as

$$\rho=\sum_{i=1}^{m}\sum_{j=1}^{n_i}\rho_{i,j}+A. \quad (3)$$

If we further assume that each nearest neighbor of the same kind has the same effect on the momentum distribution, that is, $\rho_{i,j}=\rho_{i,j'}=\rho_i$ with all j and j', Eq. (3) reduces to

$$\rho=\sum_{i=1}^{m} n_i\rho_i+A=\sum_{i=1}^{m} n_i\left(\rho_i+\frac{A}{k}\right). \tag{4}$$

Then if we have $m+1$ different vacancy complexes, we can solve the element-specific momentum distributions ρ_i and the background contribution A with Eq. (4). In practice, we can assume that the second-nearest-neighbor contribution is negligible, that is, $A \ll \rho_i$, and thus we need only m different defects to calculate the element-specific ρ_i. It should be noted that the ρ_i are distributions for an atom next to a vacancy, not that of an atom in a defect-free lattice where the positron wave function is very different.

C. Radial momentum distributions

To illustrate the changes of the momentum distribution $\Gamma(\boldsymbol{p})$, we apply the conventional analysis[35] to calculate the momentum space density of states from the experimental Doppler spectrum $I(p_z)$. In the Doppler-broadening measurement, the one-dimensional projection of the momentum distribution is measured as

$$I(p_z)=\int\int_{-\infty}^{\infty} dp_x dp_y \Gamma(\boldsymbol{p}). \tag{5}$$

We can invert this to obtain $\Gamma(\boldsymbol{p})$ if we assume that the momentum distribution is isotropic. We get for the occupation of the momentum states

$$\Gamma(p_z)=-\frac{1}{2\pi p_z}\frac{dI(p_z)}{dp_z} \tag{6}$$

and for the density of momentum states

$$N(p)=4\pi p^2\Gamma(p)=-2p\frac{dI(p)}{dp}. \tag{7}$$

This distribution goes to zero as $p\rightarrow 0$. Although Eqs. (6) and (7) are derived assuming an isotropic $\Gamma(\boldsymbol{p})$, the density of states in Eq. (7) gives illustrative information on the changes of the average electron momentum, as will be shown below. Furthermore, Eq. (7) gives a much more physical representation of changes in $\Gamma(\boldsymbol{p})$ than the more commonly used ratio or difference curves.[25,33,34,36]

IV. THEORETICAL CALCULATIONS

To support the measurements, we calculated positron lifetimes and core electron momentum distributions theoretically for different vacancy-donor complexes. We used the atomic superposition method with a 216-site supercell.[37–41] Electron-positron correlation effects in annihilation (and in the positron potential) were modeled with the generalized gradient approximation (GGA). For calculations at vacancies, two k points, Γ and L, were used. The momentum distributions were constructed of those of free atoms, which is a good approximation for core electrons. The distributions calculated in this way have been shown to be in good agreement with experiment for momentum values higher than $15\times10^{-3}m_0c$. The calculations were performed for ideal vacancies, i.e., no lattice relaxations were taken into account. The calculated momentum distributions were convoluted with the resolution of the detector system, which was 0.95 keV.

TABLE II. Positron lifetimes in different vacancy-donor complexes calculated with the atomic superposition method.

Vacancies	Donors	τ_P (ps)	τ_{As} (ps)	τ_{Sb} (ps)
0	0	207.1	207.1	207.1
1	0	241.1	241.1	241.1
1	1	244.0	241.3	234.1
1	2	246.8	241.5	226.6
1	3	249.6	241.6	219.4
1	4	252.4	241.8	213.9
2	0	300.3	300.3	300.3
2	1	302.7	301.0	296.4
2	2	305.1	301.7	292.3
2	3	307.6	302.4	288.1
2	4	310.0	303.1	283.8
2	5	312.7	303.8	279.9
2	6	315.3	304.6	275.5

Calculated lifetimes are shown in Table II. The number of vacancies in the defect complex has a clear effect on positron lifetime; the lifetime increases with increasing volume due to decreased electron density. The monovacancy lifetime is more than 30 ps higher than that of a defect-free lattice and the divacancy is about 60 ps higher than the monovacancy. The effect of donor atoms at nearest neighbors of the vacancies has clearly less of an effect than the number of vacancies. The small P atoms tend to increase the lifetime, whereas large Sb atoms decrease it. The As atoms have almost no effect.

Some of the calculated core electron momentum distributions for monovacancies are shown in Fig. 2. For pure monovacancy, the spectrum lies clearly below that of the defect-free lattice. When Si atoms next to the vacancy are replaced with P atoms, there is almost no effect on the core electron momentum distribution. This is due to the similar core electron configuration. In both cases, the core region is dominated by the $2p$ electrons. In the case of As, the distribution rises considerably with an increasing number of As atoms next to the vacancy, however the shape remains almost the same. This happens because now the core region is dominated by the ten $3d$ electrons of As instead of the six $2p$ electrons of Si and P. With Sb, there is considerable bending in the core electron momentum distribution. The core region is now dominated by the ten $4d$ electrons of Sb up to around $30\times10^{-3}m_0c$. The Sb $4d$ electrons are less localized than the As $3d$ electrons and thus have smaller momentum rising the intensity at $(15–25)\times10^{-3}m_0c$.

We also compared experimental momentum distributions with those calculated using the *ab initio* method explained in detail in Ref. 32. The results show that the effect of a mono-

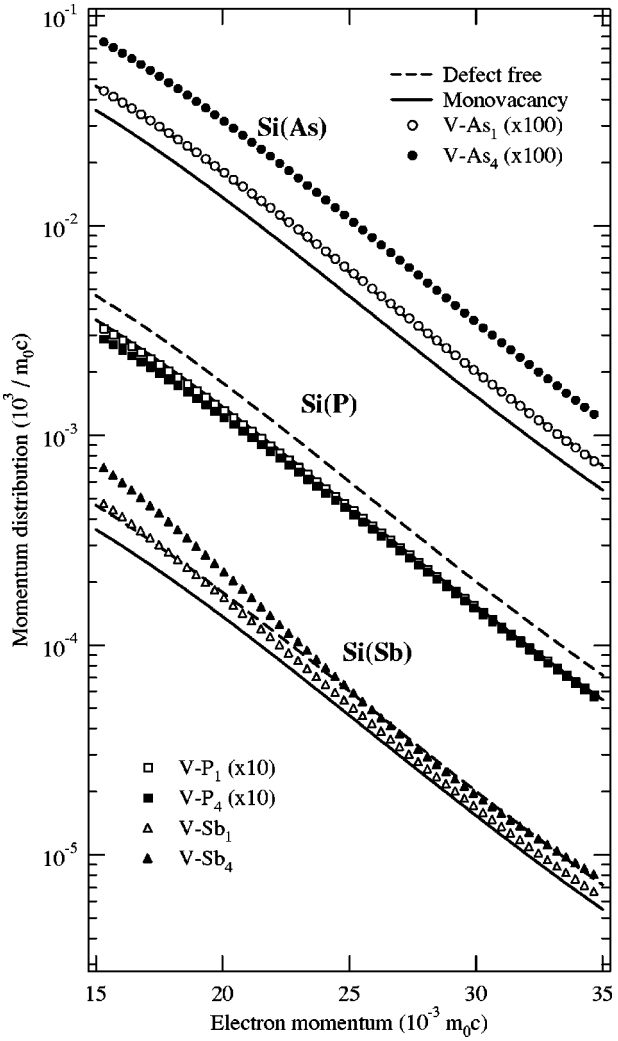

FIG. 2. Theoretical core region momentum distributions calculated with the atomic superposition method for different vacancy-donor complexes.

vacancy in the valence region is to make the momentum distribution narrower compared to defect-free distribution. The effect of As and P atoms next to a vacancy is to broaden the valence electron momentum distribution. With several As and P atoms, the spectrum gets even broader than that of the defect-free lattice. This is due to the enhanced electron density at the positive donor, increasing the momentum of the valence electrons. In the core region, the spectra agree very well with the atomic superposition results presented here in Table II and Fig. 2.

V. HIGHLY As-DOPED Si

A. Annealing of *V*-As complexes

The annealing of irradiation-induced defects in highly As-doped Si was discussed already in Ref. 26. Here we complete the experiment by studying heat treatments up to 1220 K. We also pay more attention to the details of the electron momentum distributions by applying methods described in Sec. III.

The as-grown and electron-irradiated samples before annealings were already analyzed in Ref. 25. No vacancies

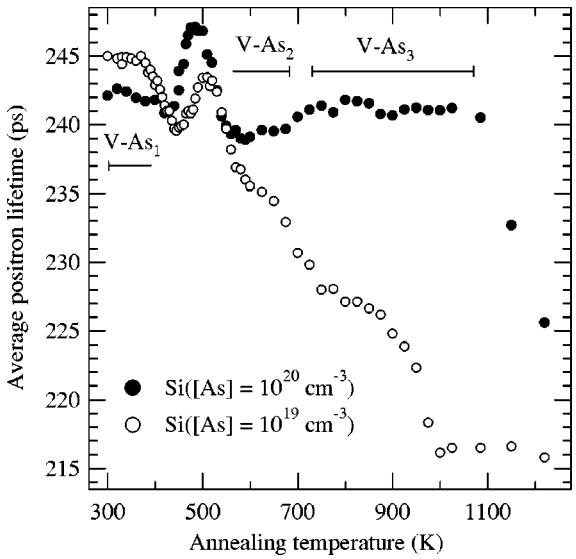

FIG. 3. Average positron lifetime as a function of annealing temperature for samples Si($[As]=10^{19}$ cm^{-3}) and Si($[As]=10^{20}$ cm^{-3}).

were found in the as-grown sample Si($[As]=10^{19}$ cm^{-3}). The as-grown Si($[As]=10^{20}$ cm^{-3}) sample was found to contain monovacancies (positron lifetime 250 ps) surrounded by three As atoms (the V-As_3 complex) at a concentration of $\sim 10^{17}$ cm^{-3}. The electron irradiation at 300 K was found to create vacancy-donor pairs (V-As_1), in good agreement with the EPR results.[42] The vacancy created by irradiation is mobile until trapped by the As atom to form the so-called E centers.[42] A small amount of divacancies was also observed. The vacancy concentration in both of the electron-irradiated samples is so high ($>10^{18}$ cm^{-3}) that all positrons annihilate as trapped at defects.

The average positron lifetime as a function of annealing temperature is shown in Fig. 3. At around 400 K, the average lifetime starts to increase. Based on the decomposition of the lifetime spectra shown in Ref. 26, the increase of the average lifetime can be attributed to divacancies formed by the dissociation of the E centers. The divacancies anneal after 500 K. At 600 K, only monovacancies are left, as shown by the decomposition of the lifetime spectra ($\tau_2 \sim 245$ ps) in Si($[As]=10^{19}$ cm^{-3}) and the presence of only a single component of ~ 240 ps in the Si($[As]=10^{20}$ cm^{-3}) sample.

The core electron momentum distributions, obtained after removing the effects of delocalized positrons in the Si lattice by positron trapping model,[36] are shown in Fig. 4. The core electron momentum distribution measured after the 600-K annealing is located clearly above the distribution in the as-irradiated sample. This is a clear indication that the number of As atoms next to the vacancy has increased since the ten As $3d$ electrons give a larger contribution to the core region spectrum than the six Si $2p$ electrons. By comparing the measured distribution with the theoretical spectrum shown in Fig. 2, the defects after 600-K annealing can be identified as V-As_2.

In the higher doped sample Si($[As]=10^{20}$ cm^{-3}), there is a small increase in the average positron lifetime at 700 K.

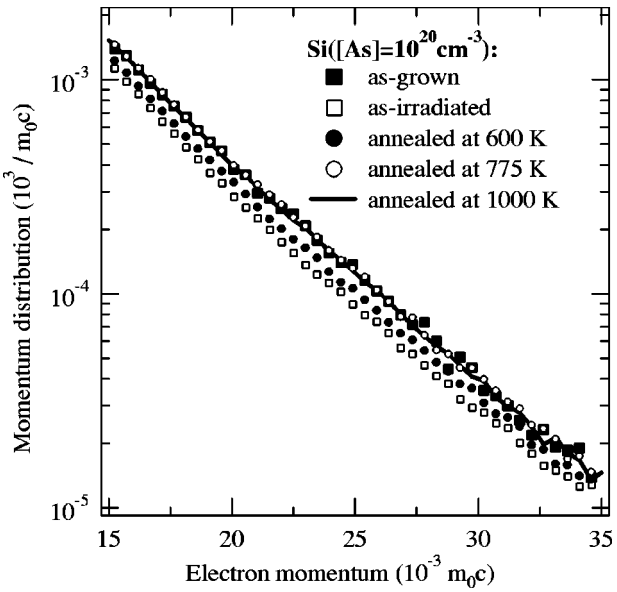

FIG. 4. Core region momentum distributions measured in sample Si($[As]=10^{20}$ cm^{-3}). In the as-grown sample, we have removed the effect from delocalized positrons with the help of measured positron lifetimes.

The coincidence Doppler measurement at 775 K shows a further rise in the core region momentum distribution (Fig. 4), indicating that more As is neighboring the vacancy than after 600-K annealing. The defects can be identified as V-As_3 by extrapolating the effect of each As atom to the core electron momentum distribution, or by direct comparison with theoretical calculations (Fig. 2).

After that, the lifetime remains constant up to 1100 K. A Doppler measurement at 1000 K gives an identical spectrum to that measured at 775 K, showing that the defects are still V-As_3 defects (Fig. 4). After 1100 K, the average positron lifetime starts to decrease rapidly and at 1220 K the lifetime has already dropped 15 ps, indicating that the defects are annealing away. The annealing of V-As_3 is seen at slightly lower temperatures in the sample with lower As doping.

The conversion of V-As_1 to V-As_2 and finally to V-As_3 can be explained by the ring diffusion mechanism.[8,10,26] The electrostatic attraction of V^- and As^+ keeps the migrating V-As_1 and V-As_2 complexes together until they are trapped by isolated As to finally form V-As_3. At high As doping of 10^{20} cm^{-3}, most of the V-As_1 are converted to V-As_2 and V-As_3 as no apparent decrease of vacancy concentration is observed (Fig. 3). The dissociations of V-As_1 and V-As_2 dominate in the sample with lower As doping since the average lifetime decreases in annealings. This is natural since an order of magnitude more migration jumps is required to form the V-As_2 and V-As_3 complexes.

As early as the 1970s, it was found that there is a heavy drop in the conductivity when highly doped Si is annealed at temperatures between 400 and 500 °C.[43–45] This deactivation of dopants was found to be partially reversible by annealing at temperatures around 800–1000 °C. The formation of V-As_3 at 700 K and its annealing at 1100 K fit these results perfectly, giving strong evidence that the V-As_3 is the deactivating defect. This observation is also in agreement with our recent results in MBE-grown Si, where the V-As_3 defects were found to anneal at 800 °C.[27]

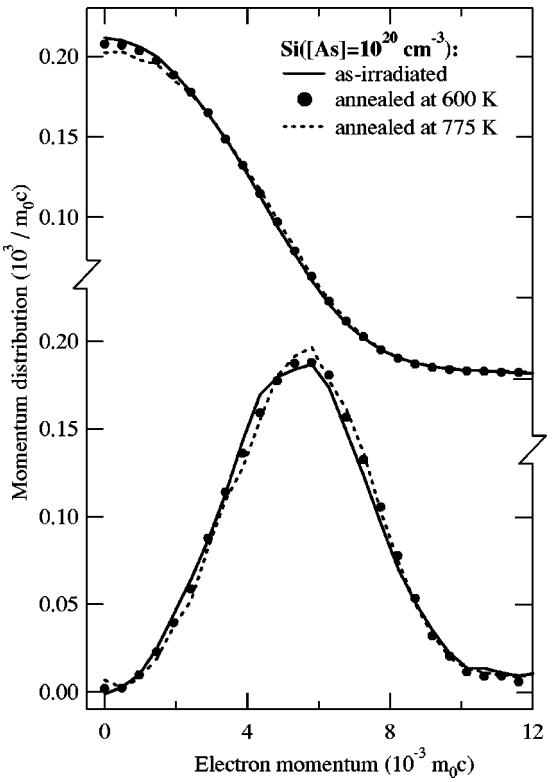

FIG. 5. Deconvoluted valence region momentum distributions measured in sample Si($[As]=10^{20}$ cm^{-3}). Also shown are densities of momentum spaces obtained with Eq. (7) (lower part of the figure).

B. Valence electron momentum distributions

The vacancy-impurity complexes can be unambiguously identified on the basis of the core electron momentum distribution. However, the momentum of the annihilating valence electrons also carries chemical information, as shown preliminarily in Ref. 25. The deconvoluted valence region spectra from sample Si($[As]=10^{20}$ cm^{-3}) are shown in Fig. 5. Compared with the as-grown sample, the presence of vacancies is clearly seen in the as-irradiated sample as a narrowing of the spectrum. The presence of V-As_2 defects at 600 K and V-As_3 at 775 K is observed as a broadening of the distributions, as seen in Fig. 5.

In Fig. 5 we also show the densities of momentum states obtained with Eq. (7). They clearly move towards higher momenta when the more As-containing defects V-As_2 and V-As_3 are formed at higher annealing temperatures. This effect has been observed earlier by applying difference curves,[25] and it is also reproduced by theoretical calculations.[25] The explanation is that the valence electron density and thus also the electron momentum near the As atom is higher than near Si due to the positive charge of the As ion. In practice, this effect is very useful for identifying vacancy-impurity pairs on the basis of their valence electron momenta, as shown below in P-doped Si (Sec. VI).

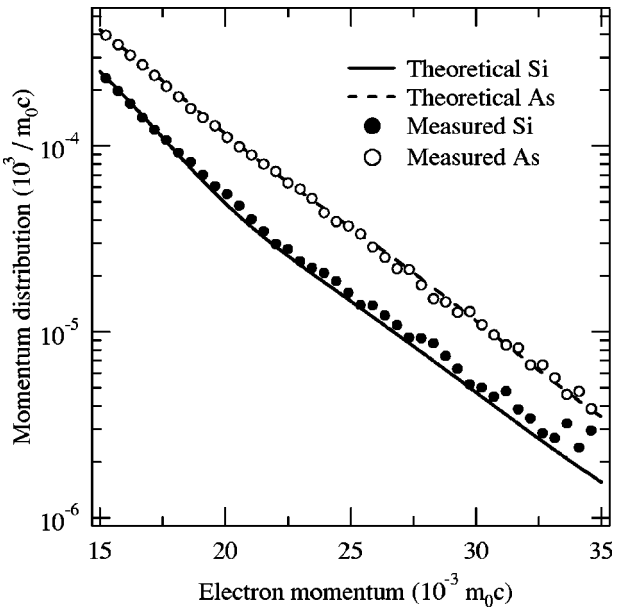

FIG. 6. The core region element-specific momentum distributions from measurements (circles) and theoretical calculations (lines).

C. Element-specific momentum distributions

The presence of one to three As atoms next to the vacancy allows us to decompose the influence of each As and Si atom to the positron-electron momentum distributions of a vacancy. Using the method explained in Sec. III B, we get for each V-As$_n$ ($n=1-3$) defect complex an equation of the form

$$\rho(V\text{-As}_n)=(4-n)\rho(\text{Si})+n\rho(\text{As}). \tag{8}$$

Since we have measured spectra from V-As$_1$, V-As$_2$, and V-As$_3$ defects, it is possible to calculate ρ(As) and ρ(Si) from three different defect complex pairs. All different combinations give similar spectra and thus only the averages are shown in Figs. 6 and 7.

We calculated the element-specific ρ(Si) and ρ(As) also from the theoretical spectra from Ref. 32 using all possible combinations (V-As$_{0-4}$). They all give almost identical results, indicating that the contribution of each As and Si atom is simply additive. This result gives strong support for the assumptions made in Sec. III B. The averages calculated from all possible combinations are shown in Fig. 7 for the valence region and in Fig. 6 for the core region.

The measured element-specific momentum distributions are in good agreement with the theoretical spectrum both in valence and core regions. The increased momentum caused by the As 3d electrons is again clearly seen in the core region (Fig. 6). Also the increased momentum in the valence region caused by the more positive As atoms is clearly seen as a much broader momentum distribution for As than for Si. The higher momentum is also seen in the densities of momentum states in Fig. 7. Thus also the valence region spectrum could be used to identify atoms around the vacancy and the element-specific distributions explain illustratively the origin of the observed changes.

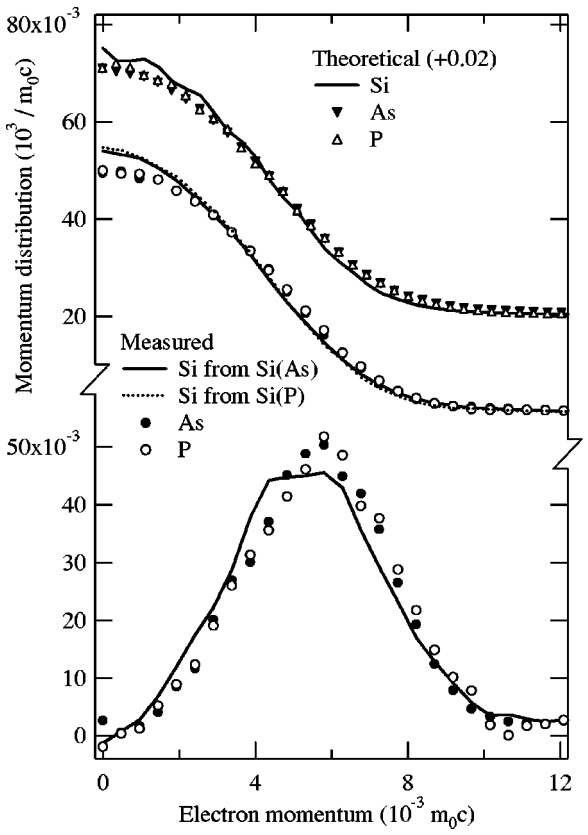

FIG. 7. The valence region element-specific momentum distributions from measurements and theoretical calculations. In the lower part of the figure are also shown the densities of momentum spaces from measurements.

VI. P-DOPED Si

A. Si with low P doping

In earlier electron paramagnetic resonance experiments, the annealing of V-As$_1$ and V-P$_1$ pairs takes place at 440 K and 400 K, respectively.[42] These experiments were typically done in lightly doped samples where it is unlikely to form V-D_n ($n\geqslant 2$) complexes by migration. To verify the simple annealing behavior of V-P$_1$ pairs, we studied lightly doped Si([P]$=3\times10^{16}$ cm^{-3}) samples after electron irradiation at 300 K.

Average positron lifetime as a function of annealing temperature is shown in Fig. 8. Since the doping, and hence also the defect concentration, is low in this sample, the positron lifetime was also measured at lower temperatures where the positron trapping to negative vacancies is enhanced and thus a clearer vacancy signal can be obtained.

Measurements at all temperatures show similar effects. After irradiation, the lifetime spectrum has two components; $\tau_2\sim250$ ps can be attributed to monovacancies (V-P$_1$ pairs) and $\tau_1=150-200$ ps to free positrons. These results are similar to ones reported previously by Mäkinen *et al.*[22] According to the simple positron trapping model,[22] the V-P$_1$ pair concentration is about 2×10^{16} cm^{-3} indicating that most P atoms are paired with a vacancy.

Between annealings at 300 and 450 K, the average lifetime decreases after which there is a similar peak as observed

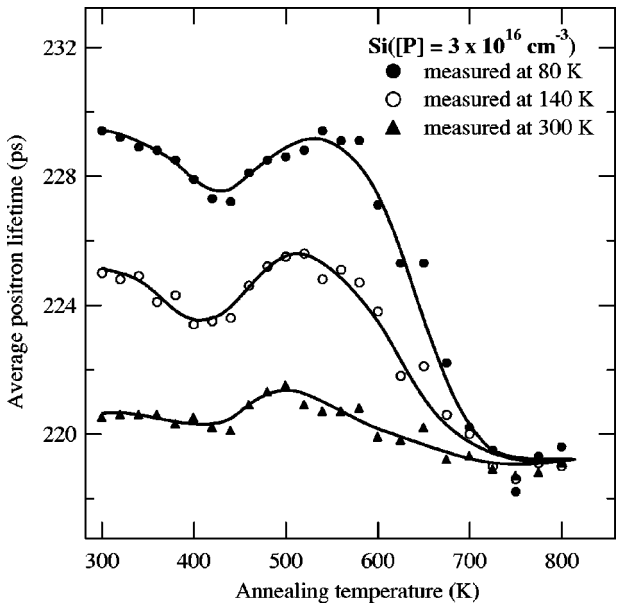

FIG. 8. Average positron lifetime measured at different temperatures as a function of annealing temperature from sample Si($[P]=3\times10^{16}$ cm^{-3}).

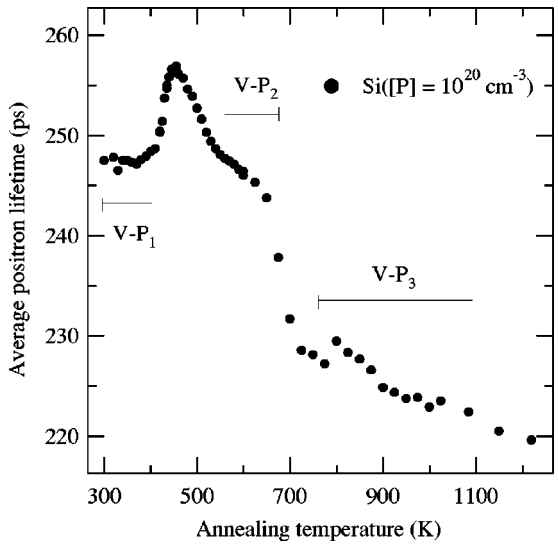

FIG. 9. Average positron lifetime as a function of annealing temperature for electron irradiated sample Si($[P]=10^{20}$ cm^{-3}).

in the highly As-doped samples (Sec. V). After the peak between 600 and 700 K, there is a rapid decrease in the lifetime, indicating that all vacancy defects anneal away.

The results show that the vacancy-phosphorus pairs created during the electron irradiation start to anneal when temperature rises above room temperature. The peak observed at 550 K can be again attributed to the formation of divacancies from the dissociating V-P_1 pairs. The rapid decrease of the average lifetime at 600–700 K indicates that both V-P_1 and V_2 defects recover away and no stable vacancy defects are left. As expected, this shows that the formation of higher-order defects, such as V-P_2 and V-P_3, does not take place at low doping concentrations of 10^{16} cm^{-3}. Notice that this is also consistent with the fact that no electrical compensation has been observed at such low P concentrations in as-grown Si.

B. Highly P-doped Si

Earlier EPR (Ref. 46) and DLTS (Ref. 47) measurements in highly P-doped Si suggest that V-P_2 defects are formed as annealing products of V-P_1 pairs. This conclusion is similar to ours in As-doped Si (Sec. V and Ref. 26). To study the complexing of vacancies and P atoms, we measured positron lifetime spectra in electron irradiated Si($[P]=10^{20}$ cm^{-3}) as a function of annealing temperature (Fig. 9). Before the annealings, the average lifetime is 248 ps, which is roughly the lifetime of a monovacancy in Si. The lifetime spectrum has a single component. We conclude, similarly to Refs. 21 and 25, that the dominant defect before annealing is the V-P_1 caused by the electron irradiation.

The average lifetime remains constant up to 400 K, after which there is a similar peak to that observed in As-doped Si and in Si($[P]=3\times10^{16}$ cm^{-3}). The peak is centered at 450 K and has a maximum value of 257 ps. The decomposition of the lifetime spectra shows again increased values of τ_2, which indicate that divacancies (300 ps) cause the average positron lifetime to increase. The divacancies are formed from the V-P_1 pairs, which start to dissociate at 400 K. Compared to the similar peak in τ_{av} in the As-doped sample, it is at 20 K lower temperature and rises 10 ps higher in the P-doped Si. This observation is consistent with the fact that V-P_1 pairs are slightly less stable than V-As_1, enabling more efficient formation of V_2.

At 450 K, the divacancies start to anneal, as observed also in Ref. 42, and at 550 K the average lifetime is back at the lifetime of a monovacancy. The lifetime spectrum has only a single component, indicating that no divacancies are left. The decrease in the average lifetime is quite slow between 550 and 650 K, and the value remains at about the lifetime of a monovacancy.

In order to identify the defects, we measured the electron momentum distributions using the Doppler-broadening technique. The spectra in the core electron region are shown in Fig. 10 and the valence region in Fig. 11. The core electron momentum distribution after 600-K annealing is almost the same as the one measured in the as-irradiated sample. Since the dominant core electrons in P are the same as in Si, namely the six $2p$ electrons, the core electron momentum distribution is very insensitive to the clustering of P atoms in the surroundings of the vacancy. This can also be seen in the theoretical momentum distributions of Fig. 2, where all V-P_{0-4} defects give almost the same spectra.

In the valence region (Fig. 11), the distribution after 600-K annealing is clearly broader than in the as-irradiated sample. The effect is the same as what was observed in the case of As doping and reproduced by theory.[25] The broadening indicates the increased presence of positive P ions next to the vacancy causing increased valence electron density, leading to increased electron momentum. The increased momentum is also seen in the density of momentum states (lower part of Fig. 11), which shifts towards higher values. Since we know from the lifetime results and core region spectra that

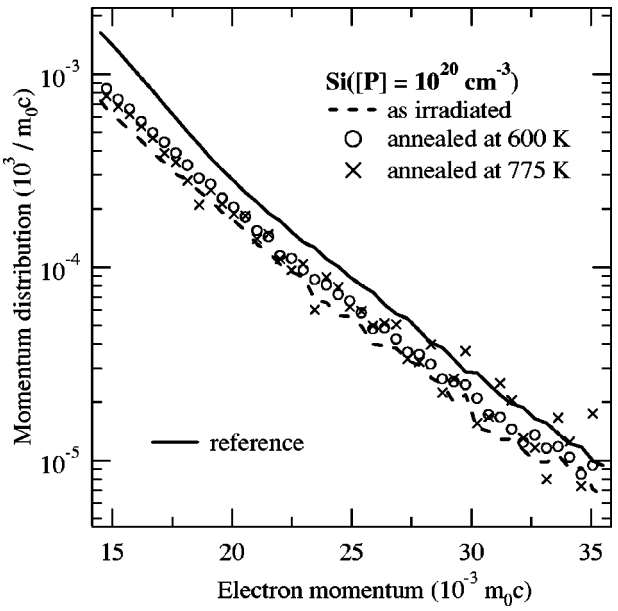

FIG. 10. Core region momentum distributions measured in sample Si($[P]=10^{20}$ cm^{-3}).

the defects are monovacancies, we can identify the defects after 600-K annealing as V-P_2. This means that around 400 K the V-P_1 pairs formed during the electron irradiation start to move and form V-P_2.

Between 650 and 700 K, the decrease in the average lifetime is fast (Fig. 9). Hence above 650 K most of the V-P_2 defects anneal away. At 700–800 K, the decomposition of the lifetime spectra indicates that the remaining defects have an open volume of a monovacancy. By applying a simple trapping model, the concentration of 5×10^{16} cm^{-3} can be estimated. Thus more than 95% of the E centers created in irradiation have disappeared but the remaining ones have formed more stable complexes.

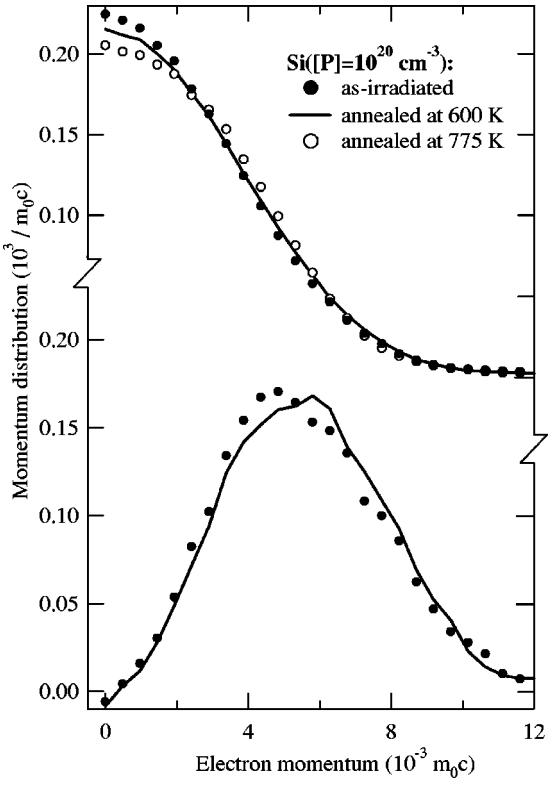

FIG. 11. Deconvoluted valence region momentum distributions from sample Si($[P]=10^{20}$ cm^{-3}). Also shown (in the lower part of the figure) are densities of momentum states.

To identify the vacancies by the electron momentum distribution measured after 775-K annealing, we remove the annihilations in the Si lattice with the help of the trapping fraction obtained from the lifetime measurements. The resulting spectrum has some scatter, especially at high momentum, but the core region of the spectrum is similar to that of a monovacancy (Fig. 10). As explained above, no effect of P atoms can be expected in these data.

The valence region distribution after 775-K annealing, on the other hand, has further broadened from the 600-K distribution (Fig. 11). Similar to the case of As doping (Fig. 5), this indicates that there are more P atoms next to the vacancy. Hence the defects after 700-K annealing can be identified as V-P_3.

The conversion of V-P_1 pairs to V-P_2 and V-P_3 complexes is similar to that observed in As-doped Si (Sec. V and Ref. 26). The ring diffusion mechanism, where electrostatic binding between the positive donor and negative vacancy is crucial, seems to explain the vacancy complex formation in P- and As-doped material. However, the dissociations seem to be more dominant in P-doped Si, since only a small fraction ($\leqslant 5\%$) of the V-P_1 pairs are finally converted to V-P_3 by annealing. This difference may be related to the lower binding energy of the P-decorated vacancy complex as manifested by the lower annealing temperatures of V-P_1 compared with that of the V-As_1 pairs.

Above 800 K, the decrease in the average lifetime is slow and at 1220 K its value is very close to that of the defect-free lattice, indicating that the defect concentration is very small. At 1000 K (not shown), the core electron momentum distribution is also very close to the spectrum measured in the defect-free sample. The concentrations of vacancy defects is thus low and V-P_3 defects obviously have recovered at 1100 K.

C. Element-specific momentum distributions

We decomposed the element-specific contributions of Si and P atoms to the electron momentum distributions as explained in Sec. III B. The decomposition was done using the as-irradiated spectrum (V-P_1 defects) and 600-K annealed spectrum (V-P_2 defects). The element-specific momentum distributions of As and P atoms are shown in Fig. 7 in the valence region.

The figure shows that the measured spectra are very similar to the theoretical ones. Both P and As donor atoms show the similar broadening due to the enhanced electron density, as expected from theory. The associated shift of the density of states to higher momenta is notable. The element-specific momentum distribution of the Si atom is obtained similarly from both P-doped (V-P_n complexes) and As-doped (V-As_n

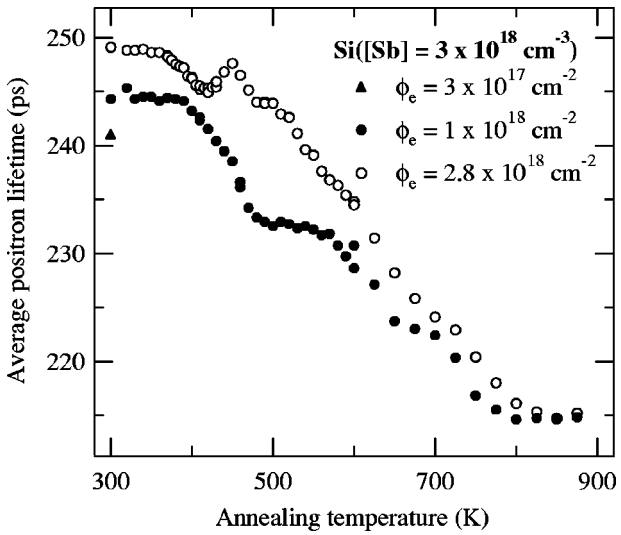

FIG. 12. Average positron lifetime as a function of annealing temperature from the electron irradiated Si($[Sb]=3\times10^{18}$ cm^{-3}) samples.

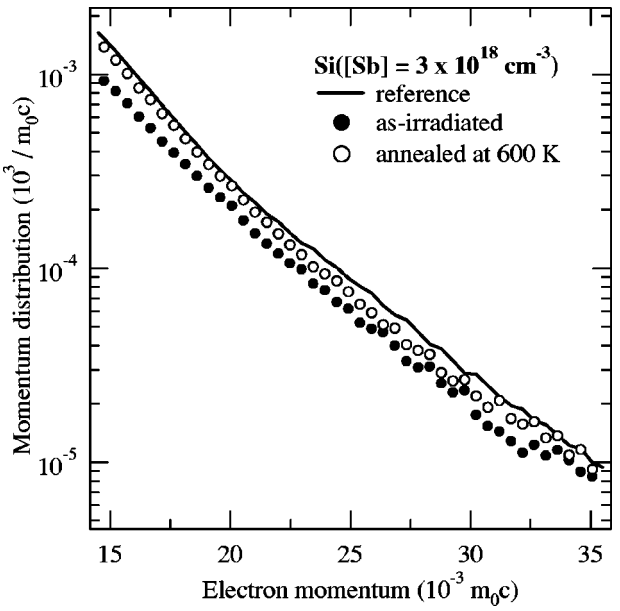

FIG. 13. Core region momentum distributions measured in Si($[Sb]=3\times10^{18}$ cm^{-3}) sample with the highest irradiation dose.

complexes) samples. This indicates again that the superposition of atom-specific momentum distributions is indeed linear.

VII. Sb-DOPED Si

Highly Sb-doped Si has attracted a lot of attention recently due to the high contrast of Sb atoms in images recorded by scanning transmission electron microscopy.[17] Dopant atom pairs were detected in samples grown by MBE at low temperatures ($T\approx550$ K) but the presence of vacancies next to the Sb pairs has not been verified. As demonstrated above for As and P doping, electron irradiation experiments followed by annealing reveal annealing mechanisms and stabilities of vacancy-impurity complexes. This fundamental information can be used, e.g., to determine which defects are stable at the epitaxial growth temperatures.

The measurements were made in three different sample pairs with identical doping [Si($[Sb]=3\times10^{18}$ cm^{-3})] but with different irradiation doses: 3×10^{17} cm^{-2}, 1.0×10^{18} cm^{-2}, and 2.8×10^{18} cm^{-2}. The average positron lifetimes measured in these samples as a function of annealing temperature are shown in Fig. 12.

Before the annealings, the lifetimes are roughly that of a monovacancy, the lifetime of the most irradiated sample being about 5 and 8 ps higher than in the other samples, namely 250 ps. The average lifetime is almost the same for all irradiation doses, indicating saturation of positron trapping. Similarly to As- and P-doped Si, we attribute the majority of the defects to the irradiation-induced V-Sb_1 pairs. The Sb concentrations of our samples are clearly less than those of the As- and P-doped ones in Secs. V and VI B. Thus the relative fraction of divacancies could be higher, explaining the slightly higher average positron lifetime and its dependence on the irradiation dose.

After 380-K annealing, the average lifetimes start to decrease. In the sample with the highest irradiation dose, there is a peak in the average lifetime at 460 K. This peak is again attributed to the formation and annealing of divacancies created from the dissociating E centers. The peak is much smaller than in the As- and P-doped samples. Since V-Sb_1 pairs are more stable than V-P_1 or V-As_1 pairs, fewer divacancies can form in the annealing and the created V_2 defects are stable only in the narrow temperature range around 450 K.

In the sample with the irradiation dose of 1×10^{18} cm^{-2}, the positron lifetime remains constant between 450 and 550 K. The lifetime is 233 ps, which is about 12 ps less than before the annealings. In the most irradiated sample ($\phi_e=2.8\times10^{18}$ cm^{-2}) there is no clear constant lifetime region; the lifetime continues to decrease after the small peak at 450 K. The monovacancies are expected to be the same as in the less irradiated sample and the decrease of lifetime comes mostly from the annealing of divacancies.

To identify the defects, coincidence Doppler measurements were made in as-irradiated and 600-K annealed samples. The core region momentum distributions are shown in Fig. 13 and the valence region in Fig. 14. In the distribution after annealing at 600 K, the effect of delocalized positrons is removed with the help of the positron lifetime results.

In the core electron region, the spectrum in the 600-K annealed sample has larger intensity than that of the as-irradiated sample. The spectrum has also clearly bended so that the difference to the as-irradiated momentum distribution is smallest at $(20-25)\times10^{-3}m_0c$. This bending, which is also seen in the theoretical spectra in Fig. 2, is attributed to the increased presence of Sb $4d$ electrons. This means that in the annealings at 500–600 K, some of the V-Sb_1 pairs are converted to V-Sb_2 defects.

In the valence electron region, the spectrum after 600-K annealing is broader than in the as-irradiated sample (Fig. 14). The densities of momentum states (Fig. 14) show the

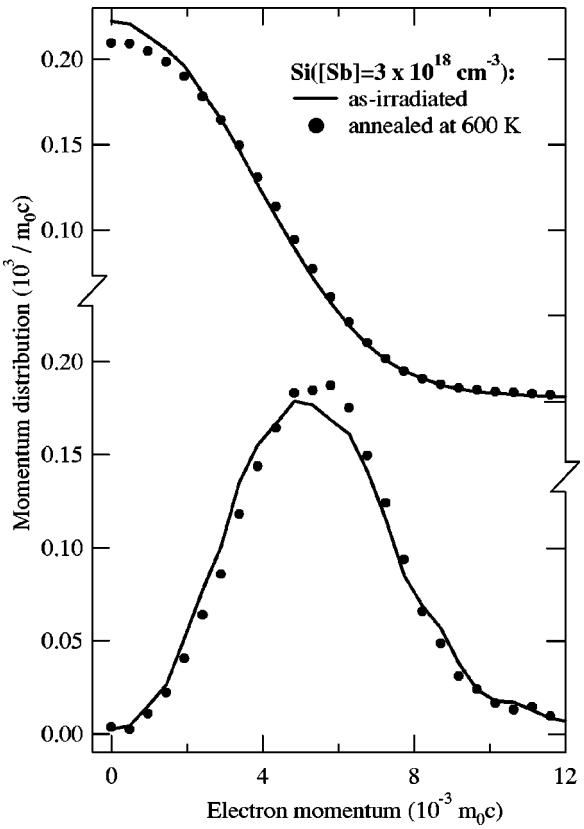

FIG. 14. Deconvoluted valence region momentum distributions and densities of momentum states measured in Si([Sb]$=3\times10^{18}$ cm^{-3}) sample with higher irradiation dose.

same effect: the peak moves to higher momentum. Similar to the case of P and As doping (Secs. V and VI B), this is attributed to increased electron density near the positive Sb ion. Thus also the valence region momentum distribution supports the conclusion that the number of Sb around the vacancy has increased, most likely to two (i.e., the defect is V-Sb_2). The formation of V-Sb_2 defects can be explained with similar ring diffusion mechanisms to those above in the case of P and As doping.

After 600 K, the annealing behaviors of the two irradiated samples are similar. The lifetime continues to decrease until it reaches the defect-free level at 800 K. This indicates that the donor concentration is too small to create substantial concentrations of defect complexes which are stable at higher temperatures, such as V-Sb_3.

VIII. CONCLUSIONS

We have studied the annealing of electron-irradiation-induced defects in highly As-, P-, and Sb-doped Si. The electron irradiation creates vacancy-donor pairs (V-D_1) which start to migrate at 400–450 K. The migrating and dissociating V-D_1 defects form more stable V-D_2 defects and some divacancies. The divacancies start to anneal away soon after they are formed, around 450–500 K, and at 600 K there are only V-D_2 defects left.

In the case of As and P doping, the V-D_2 defects start to migrate at 650–700 K forming V-D_3 defects. The formation of V-D_2 and V-D_3 depends heavily on the doping concentration. In the case of As at the doping of 10^{20} cm^{-3}, most V-As_2 defects are converted to V-As_3 defects after 800-K annealing, whereas at 10^{19} cm^{-3} about 90% of the V-As_2 complexes dissociate. In the case of P doping, not even a concentration of 10^{20} cm^{-3} is enough for complete conversion to V-P_3. In the Sb-doped samples, the doping concentrations were much smaller (3×10^{18} cm^{-3}) and no clear evidence of V-Sb_3 could be obtained.

Our results indicate that the formation of V-D_2 and V-D_3 defects from irradiation induced V-D_1 pairs is qualitatively similar for P, As, and Sb dopants. The vacancy-impurity complexing in all these cases can be explained by the ring diffusion mechanism, where the opposite charges of the vacancy and the donor atom bind the migrating complex together.

We observed also the recovery of V-As_3 defects after 1100-K annealing. The formation of V-D_3 defects at 700 K and their annealing at 1100 K are in perfect agreement with the well-known properties of the electrical compensation in highly doped Si. The observed decrease of free-electron concentration after heat treatment at 700–800 K and subsequent reactivation of doping at 1100–1300 K can thus be explained by the formation and annealing of the V-D_3 defects.

We have also shown that the deconvoluted valence region positron-electron momentum distribution can be a valuable aid in the identification of atoms next to a vacancy. By further calculating the density of momentum states, changes in the momenta of the valence electrons can be observed. These changes serve as fingerprints of different atoms at nearest-neighbor sites and thus can help in the defect identification. We show that element-specific momentum distributions can be determined and the effect of individual atoms to the momentum distribution can be extracted.

[1] A. Nylandsted Larsen, F.T. Pedersen, G. Weyer, R. Galloni, R. Rizzoli, and A. Armigliato, J. Appl. Phys. **59**, 1908 (1986).
[2] H.-J. Gossmann, F.C. Unterwald, and H.S. Luftman, J. Appl. Phys. **73**, 8237 (1993).
[3] H.H. Radamson, J.M.R. Sardela, L. Hultman, and G.V. Hansson, J. Appl. Phys. **76**, 763 (1994).
[4] A. Nylandsted Larsen, K.K. Larsen, and P.E. Andersen, J. Appl. Phys. **73**, 691 (1993).
[5] J.L. Allain, J.R. Regnard, A. Bourret, A. Parisini, A. Armigliato, G. Tourillon, and S. Pizzini, Phys. Rev. B **46**, 9434 (1992).
[6] C. Revenant-Brizard, J.R. Regnard, S. Solmi, A. Armigliato, S. Valmorri, C. Cellini, and F. Romanato, J. Appl. Phys. **79**, 9037 (1996).
[7] K.C. Pandey, A. Erbil, I.G.S. Cargill, R.F. Boehme, and D. Vanderbilt, Phys. Rev. Lett. **61**, 1282 (1988).
[8] M. Ramamoorthy and S.T. Pantelides, Phys. Rev. Lett. **76**, 4753 (1996).
[9] D. Mathiot and J.C. Pfister, J. Appl. Phys. **66**, 970 (1989).

[10] J. Xie and S.P. Chen, Phys. Rev. Lett. **83**, 1795 (1999).
[11] M.A. Berding, A. Sher, M. van Schilfgaarde, P.M. Rousseau, and W.E. Spicer, Appl. Phys. Lett. **72**, 1492 (1998).
[12] A. Nylandsted Larsen, P. Kringhøj, J. Lundsgaard Hansen, and S.Yu. Shiryaev, J. Appl. Phys. **81**, 2173 (1997).
[13] D.W. Lawther, U. Myler, P.J. Simpson, P.M. Rousseau, P.B. Griffin, and J.D. Plummer, Appl. Phys. Lett. **67**, 3575 (1995).
[14] U. Myler, R.D. Goldberg, A.P. Knights, D.W. Lawther, and P.J. Simpson, Appl. Phys. Lett. **69**, 3333 (1996).
[15] S. Szpala, P. Asoka-Kumar, B. Nielsen, J.P. Peng, S. Hayakawa, K.G. Lynn, and H.-J. Gossmann, Phys. Rev. B **54**, 4722 (1996).
[16] D.J. Chadi, P.H. Citrin, C.H. Park, D.L. Adler, M.A. Marcus, and H.-J. Gossmann, Phys. Rev. Lett. **79**, 4834 (1997).
[17] P.M. Voyles, D.A. Muller, J.L. Grazul, P.H. Citrin, and H.-J.L. Gossmann, Nature (London) **416**, 826 (2002).
[18] P.M. Voyles, D.J. Chadi, P.H. Citrin, D.A. Muller, J.L. Grazul, P.A. Northrup, and H.-J.L. Gossmann, Phys. Rev. Lett. **91**, 125505 (2003).
[19] G.D. Watkins and J.W. Corbett, Phys. Rev. **134**, A1359 (1964).
[20] E.L. Elkin and G.D. Watkins, Phys. Rev. **174**, 881 (1968).
[21] J. Mäkinen, C. Corbel, P. Hautojärvi, P. Moser, and F. Pierre, Phys. Rev. B **39**, 10 162 (1989).
[22] J. Mäkinen, P. Hautojärvi, and C. Corbel, J. Phys.: Condens. Matter **4**, 5137 (1992).
[23] A. Polity, F. Börner, S. Huth, S. Eichler, and R. Krause-Rehberg, Phys. Rev. B **58**, 10 363 (1998).
[24] V. Avalos and S. Dannefaer, Phys. Rev. B **58**, 1331 (1998).
[25] K. Saarinen, J. Nissilä, H. Kauppinen, M. Hakala, M.J. Puska, P. Hautojärvi, and C. Corbel, Phys. Rev. Lett. **82**, 1883 (1999).
[26] V. Ranki, J. Nissilä, and K. Saarinen, Phys. Rev. Lett. **88**, 105506 (2002).
[27] V. Ranki, K. Saarinen, J. Fage-Pedersen, J. Lundsgaard Hansen, and A. Nylandsted Larsen, Phys. Rev. B **67**, 041201 (2003).
[28] H. Kauppinen, C. Corbel, J. Nissilä, K. Saarinen, and P. Hautojärvi, Phys. Rev. B **57**, 12 911 (1998).
[29] M.J. Puska, C. Corbel, and R.M. Nieminen, Phys. Rev. B **41**, 9980 (1990).
[30] K. Shizuma, Nucl. Instrum. Methods **150**, 447 (1978).
[31] J.C. Erskine and J.D. McGervey, Phys. Rev. **151**, 615 (1966).
[32] M. Hakala, M.J. Puska, and R.M. Nieminen, Phys. Rev. B **57**, 7621 (1998).
[33] P. Asoka-Kumar, M. Alatalo, V.J. Ghosh, A.C. Kruseman, B. Nielsen, and K.G. Lynn, Phys. Rev. Lett. **77**, 2097 (1996).
[34] M. Biasini, G. Ferro, P. Folegati, and G. Riontino, Phys. Rev. B **63**, 092202 (2001).
[35] A.T. Stewart, Can. J. Phys. **35**, 168 (1957).
[36] R. Krause-Rehberg and H.S. Leipner, *Positron Annihilation in Semiconductors* (Springer, Berlin, 1999).
[37] M. Alatalo, H. Kauppinen, K. Saarinen, M.J. Puska, J. Mäkinen, P. Hautojärvi, and R.M. Nieminen, Phys. Rev. B **51**, 4176 (1995).
[38] M. Alatalo, B. Barbiellini, M. Hakala, H. Kauppinen, T. Korhonen, M.J. Puska, K. Saarinen, P. Hautojärvi, and R.M. Nieminen, Phys. Rev. B **54**, 2397 (1996).
[39] B. Barbiellini, M.J. Puska, T. Torsti, and R. Nieminen, Phys. Rev. B **51**, 7341 (1995).
[40] B. Barbiellini, M.J. Puska, T. Korhonen, A. Harju, T. Torsti, and R. Nieminen, Phys. Rev. B **53**, 16 201 (1996).
[41] M.J. Puska and R.M. Nieminen, J. Phys. F: Met. Phys. **13**, 333 (1983).
[42] G.D. Watkins, in *Deep Centers in Semiconductors*, edited by S. T. Pantelides (Gordon and Breach, London, 1986).
[43] A. Lietoila, J.F. Gibbons, and T.W. Sigmon, Appl. Phys. Lett. **36**, 765 (1980).
[44] W.-K. Chu, Appl. Phys. Lett. **36**, 273 (1980).
[45] R.O. Schwenker, E.S. Pan, and R.F. Lever, J. Appl. Phys. **42**, 3195 (1971).
[46] E.G. Sieverts and C.A.J. Ammerlaan, Inst. Phys. Conf. Ser. **31**, 213 (1977).
[47] A. Nylandsted Larsen, C. Christensen, and J.W. Petersen, J. Appl. Phys. **86**, 4861 (1999).